Journal of Radiology and Imaging

Iwasaki A et al., J Radiol Imaging. 2024, 8(2):4-10
http://dx.doi.org/10.14312/2399-8172.2024-2

NobleResearch
An Open Access Publisher
www.nobleresearch.org

Original research

Open Access

Consideration for a revised Gaussian-pencil-beam-model reported for calculation of the in-water dose caused by clinical electron-beam irradiation

Akira Iwasaki[1,*], Shingo Terashima[2,*], Shigenobu Kimura[3], Kohji Sutoh[3], Kazuo Kamimura[3], Yoichiro Hosokawa[2] and Masanori Miyazawa[4]

[1]2-3-24 Shimizu, Hirosaki, Aomori 036-8254, Japan
[2]Graduate School of Health Sciences, Hirosaki University, 66-1 Hon-cho, Hirosaki, Aomori 036-8564, Japan
[3]Department of Radiology, Aomori City Hospital, 1-14-20 Katta, Aomori 030-0821, Japan
[4]Technology of Radiotherapy Corporation, 2-1-2 Koishikawa, Bunkyo-ku, Tokyo 175-0092, Japan

Abstract

Purposes: We perform further development for our previous Gaussian-pencil-beam-model used for calculating the electron dose in water under clinical electron-beam irradiation. The main purpose is to evaluate accurately the parallel beam depth-doses at deep depths beyond about the extrapolated range (R_p) under an infinite field. *Methods:* Sets of parallel beam depth-doses under an infinite field were reconstructed for the same beams of E=6, 12, and 18 MeV in light of the electron Monte Carlo (eMC) datasets as reported by Wieslander and Knöös (2006), separating the datasets into the direct electron beam and direct-plus-indirect electron beam groups. Particularly, for each electron beam, we took serious views of the depth-dose (DD) curves near the beam entrance surface and of the OAD (off-axis dose) curves at deep depths beyond about the extrapolated range (R_p) under an infinite field. *Results and conclusions:* The following results were obtained by comparing the calculated DD and OAD datasets with the eMC datasets: (i) The revised Gaussian pencil beam model is of practical use without using complicated correction factors; and (ii) The DD and OAD datasets are yielded effectively over wide ranges of depths and off-axis distances, respectively.

Keywords: Gaussian pencil beam model; dose calculation; electron MC; electron beams; linear accelerator

Research highlights

The dose caused by the clinical electron-beam irradiation is mainly composed of the doses due to the direct electrons, the indirect electrons, and the contaminant photons. In light of the electron Monte Carlo (eMC) datasets reported by Wieslander and Knöös (2006), the present paper describes further development of the Gaussian-pencil-beam-model for calculating doses in a homogeneous water phantom for direct electron beams and direct-plus-indirect electron beams. The study subjects are how to calculate dose-datasets accurately both near the beam entrance surface and at deep depths. Accurate datasets of depth-dose (DD) and off-axis dose (OAD) were obtained from the shallow to deep depths for each of the electron beams.

1. Introduction

Wieslander and Knöös [1, 2] have reported characteristic features of the dose in homogeneous water, caused by clinical electron-beam irradiations, using an electron Monte Carlo (eMC) method for 6-, 12-, and 18-MeV electron beams by taking 10×10 cm^2 and 10×10/14×14 cm^2 applicators. The 10×10 cm^2 applicator is used for the 6- and 18-MeV electron beams, and the 10×10/14×14 cm^2 applicator is used for the 12-MeV electron beams setting a lead plate opening of 10×10 cm^2 in the 14×14 cm^2 applicator. The dose studies are classified into three categories: (a) datasets caused by contaminant photons from the treatment head, (b) datasets caused by direct electrons that have not interacted in the electron applicator, and (c) datasets caused by indirect electrons that have interacted in the electron applicator. For each group of the 6-, 12-,

***Corresponding authors:** Akira Iwasaki, 2-3-24 Shimizu, Hirosaki, Aomori 036-8254, Japan. Tel.: +172-33-2480; Email: fmcch384@ybb.ne.jp, and Shingo Terashima, Graduate School of Health Sciences, Hirosaki University, 66-1 Hon-cho, Hirosaki, Aomori 036-8564, Japan. Tel.: +81-172-39-5525; Email: s-tera@hirosaki-u.ac.jp

Received 28 March 2024 *Revised* 20 May 2024 *Accepted* 30 May 2024 *Published* 8 June 2024

Citation: Iwasaki A, Terashima S, Kimura S, Sutoh K, Kamimura K, Hosokawa Y, Miyazawa M. Consideration for a revised Gaussian-pencil-beam-model reported for calculation of the in-water dose caused by clinical electron-beam irradiation. J Radiol Imaging. 2024; 8(2):4-10. DOI: 10.14312/2399-8172.2024-2

and 18-MeV electron beams, the study work is performed using two eMC algorithms by setting a common virtual accelerator; one is that developed by them as the standard eMC, and the other is a commercial treatment planning system (TPS). The present paper refers to these datasets as "the W-K eMC dose datasets" or "the W-K eMC dose work."

The eMC treatment is usually a time-consuming work. Iwasaki and others [3, 4] have reported papers to recalculate the W-K eMC dose datasets using an analytical method to shorten the treatment time. However, the reported papers have the following defects:

- Both the depth-dose (DD) datasets and the off-axis dose (OAD) datasets were inaccurately calculated in the region near the beam entrance surface by taking unreasonable calculation procedures for calculation of the S_c^{eff} factor.
- Parallel-beam depth-dose datasets (D_∞) of infinite field were not precisely estimated at deep depths beyond about the extrapolated range (R_p).
- Each set of the OAD profiles was not reconstructed by taking account of the balanced forms at deep depths.

This paper will report how these three problems are overcome for calculating doses more precisely using a mathematical analysis for a simplified homogenous water phantom, preparing future studies how to calculate doses also analytically keeping high accuracy even for heterogeneous phantoms.

2. Methods

We describe this section based on the electron beam DD and OAD datasets of the W-K eMC dose work [2]. As described above, each of the DD and OAD datasets is yielded by setting a common virtual accelerator for both of the standard eMC and the TPS eMC. Here, it should be emphasized that each of the DD and OAD datasets is normalized with a dose of 1.0 Gy per 100 MU at the maximum dose depth (d_{max}) yielded by all particles of contaminant photons, direct electrons, and indirect electrons under the use of an open electron applicator of A_{appl}=20×20 cm^2. We use the same dose unit of Gy/100MU for each of the DD and OAD datasets. Here, in this paper, the "no unit" means a constant value when the factor is set exponentially and used for multiplication with the Z_c-axis in cm.

2.1. DD and OAD datasets

First, we describe how each of the electron beam DD and OAD datasets is expressed using a set of expressions for the direct electron beams and for the direct-plus-indirect electron beams. As listed in Table 1, we use the same *KK* numbers of *KK*=1 to 24 for the DD and OAD datasets published in the W-K paper of Ref. [2], as originally introduced in the previous papers [3, 4], also indicating the beam energy (*E*), the electron applicator (A_{appl}), and the standard or TPS eMC. It should be noted that each of the OAD datasets is yielded on two horizontal planes at shallow or deep Z_c depth (we specify the two depths as Z_1 and Z_2, respectively), and that, although each DD dataset has no *KK* number directly, it is used in common with the corresponding two OAD datasets. Namely, the *KK* numbers also indicate the corresponding diagrams used in the W-K paper (*Supp. Fig.* 3a & 3b, etc.).

Table 1 Datasets of $a_1'(E)$, $b_1'(E)$, $a_1(E)$, $b_1(E)$, and $c_1(E)$ for (a) *KK*=1-12 (direct electron beams) and (b) for *KK*=13-24 (direct-plus-indirect electron beams), related with the beam energy (*E*), the applicator (A_{appl}), the standard or TPS eMC, and the *figure number* as compiled in the W-K paper 2.

Table 1a For the direct electron beams (*KK*=1-12).

W-K datasets (KK=1-12)	*E (MeV)*	A_{appl} *(cm²)*	$a_1'(E)$ *(cm)*	$b_1'(E)$ (no unit)	$a_1(E)$ *(cm)*	$b_1(E)$ *(no unit)*	$c_1(E)$ *(no unit)*
(i) Using the standard eMC (in stepped curves)							
KK=1 & 2 for fig. 3(a)-(c)	6	10×10	10.60	1.96E-01	3.52E-08	19.72	9.80E-03
KK=3 & 4 for fig. 5(a)-(c)	12	10×10/14×14	10.55	4.07E-02	3.45E-19	44.77	8.45E-03
KK=5 & 6 for fig. 3(d)-(f)	18	10×10	10.58	2.46E-02	3.71E-23	53.73	8.50E-03
(ii) Using the TPS eMC (in dotted curves)							
KK=7 & 8 for fig. 3(a)-(c)	6	10×10	10.60	2.31E-01	2.28E-07	17.89	9.83E-03
KK =9 & 10 for fig. 5(a)-(c)	12	10×10/14×14	10.55	3.97E-02	1.95E-15	36.15	9.46E-03
KK=11 & 12 for fig. 3(d)-(f)	18	10×10	10.58	2.46E-02	1.70E-23	54.50	8.50E-03

Table 1a is constructed for the direct electron beams:

(i) The standard eMC datasets are classified into:

Under the DD dataset in *Supp. Fig.* 3a, we set *KK*=1 for *Supp. Fig.* 3b-OAD (Z_1=1 cm) and set *KK*=2 for *Supp. Fig.* 3c-OAD (Z_2=5 cm);

Under the DD dataset in *Supp. Fig.* 5a, we set *KK*=3 for *Supp. Fig.* 5b-OAD (Z_1=2 cm) and set *KK*=4 for *Supp. Fig.* 5c-OAD (Z_2=10 cm);

Under the DD dataset in *Supp. Fig.* 3d, we set *KK*=5 for *Supp. Fig.* 3e-OAD (Z_1=3 cm) and set *KK*=6 for *Supp. Fig.* 3f-OAD (Z_2=15 cm).

(ii) The TPS eMC datasets are classified into:

Under the DD dataset in *Supp. Fig.* 3a, we set *KK*=7 for *Supp. Fig.* 3b-OAD (Z_1=1 cm) and set *KK*=8 for *Supp. Fig.* 3c-OAD (Z_2=5 cm);

Under the DD dataset in *Supp. Fig.* 5a, we set *KK*=9 for *Supp. Fig.* 5b-OAD (Z_1=2 cm) and set *KK*=10 for *Supp. Fig.* 5c-OAD (Z_2=10 cm);

Under the DD dataset in *Supp. Fig.* 3d, we set *KK*=11 for *Supp. Fig.* 3e-OAD (Z_1=3 cm) and set *KK*=12 for *Supp. Fig.* 3f-OAD (Z_2=15 cm).

Table 1b For the direct-plus-indirect electron beams (*KK*=13-24).

W-K datasets (KK=13-24)	*E (MeV)*	A_{appl} *(cm²)*	$a'_1(E)$ *(cm)*	$b'_1(E)$ *(no unit)*	$a_1(E)$ *(cm)*	$b_1(E)$ *(no unit)*	$c_1(E)$ *(no unit)*
(i) Using the standard eMC (in stepped curves)							
KK=13 & 14 for fig. 3(a)-(c)	6	10×10	10.60	2.34E-01	3.72E-07	17.40	9.86E-03
KK=15 & 16 for fig. 5(a)-(c)	12	10×10/14×14	10.55	4.07E-02	1.52E-22	52.45	8.56E-03
KK=17 & 18 for fig. 3(d)-(f)	18	10×10	10.58	2.46E-02	3.17E-23	53.88	8.50E-03
(ii) Using the TPS eMC (in dotted curves)							
KK=19 & 20 for fig. 3(a)-(c)	6	10×10	10.60	2.31E-01	2.02E-07	18.01	9.88E-03
KK=21 & 22 for fig. 5(a)-(c)	12	10×10/14×14	10.55	4.11E-02	3.28E-16	37.95	8.37E-03
KK=23 & 24 for fig. 3(d)-(f)	18	10×10	10.58	2.46E-02	7.13E-24	55.36	8.50E-03

Table 1b is constructed for the direct-plus-indirect electron beams:

(i) The standard eMC datasets are classified into:

Under the DD dataset in *Supp. Fig.* 3a, we set *KK*=13 for *Supp. Fig.* 3b-OAD (Z_1=1 cm) and set *KK*=14 for *Supp. Fig.* 3c-OAD (Z_2=5 cm);

Under the DD dataset in *Supp. Fig.* 5a, we set *KK*=15 for *Supp. Fig.* 5b-OAD (Z_1=2 cm) and set *KK*=16 for *Supp. Fig.* 5c-OAD (Z_2=10 cm);

Under the DD dataset in *Supp. Fig.* 3d, we set *KK*=17 for *Supp. Fig.* 3e-OAD (Z_1=3 cm) and set *KK*=18 for *Supp. Fig.* 3f-OAD (Z_2=15 cm).

(ii) The TPS eMC datasets are classified into:

Under the DD dataset in *Supp. Fig.* 3a, we set *KK*=19 for *Supp. Fig.* 3b-OAD (Z_1=1 cm) and set *KK*=20 for *Supp. Fig.* 3c-OAD (Z_2=5 cm);

Under the DD dataset in *Supp. Fig.* 5a, we set *KK*=21 for *Supp. Fig.* 5b-OAD (Z_1=2 cm) and set *KK*=22 for *Supp. Fig.* 5c-OAD (Z_2=10 cm);

Under the DD dataset in *Supp. Fig.* 3d, we set *KK*=23 for *Supp. Fig.* 3e-OAD (Z_1=3 cm) and set *KK*=24 for *Supp. Fig.* 3f-OAD (Z_2=15 cm).

2.2. Effective field side (S_c^{eff})

In the previous papers [3, 4], we made mistakes for setting effective fields of $A_c^{eff} = S_c^{eff}$ X S_c^{eff} at shallow depths of $Z_c < Z_1$. Although no large dose errors happen in the DD curves at Z_c depths beyond about 1E-05 cm for each beam energy of E=6, 12, and 18 MeV, the OAD curve forms gradually narrower widths as the Z_c depth decreases from each Z_1 depth as indicated in Ref. [4]. The present paper proposes another treatment for the A_c^{eff} field at depths of $Z_c < Z_1$. Here, we express the effective field side (S_c^{eff}) for each beam as a function of Z_c for a given beam energy (E). We use functional expressions of $S_c^{eff}(Z_c)$ and $S_c^{eff}(Z_c, E)$ case by case.

For the blue lines, as illustrated in Figure 1, we set S_c^{eff} (0) on the beam entrance surface (Z_c = 0), where we simply set the value of $S_c^{eff}(0)$ as the field side determined using the geometry of the fan beam coming out from the electron applicator by the use of the effective source-to-surface distance of SSD_{eff} [3]. Then we set $S_c^{eff}(Z_1)$ for the depth of $Z_c = Z_1$, and set $S_c^{eff}(Z_2)$ for the depth of $Z_c = Z_2$. [we can set $S_c^{eff}(Z_c = 0) < S_c^{eff}(Z_c = Z_1)$ holding $S_c^{eff}(Z_c = 0) \cong S_c^{eff}(Z_c = Z_1)$].

Table 2 (composed of Tables 2a to 2d) lists S_c^{eff} datasets for both standard eMC and the TPS eMC. It should be noted that the S_c^{eff} (0) values are almost constant (10.5 or 10.6 cm) for each irradiation because of a simplified treatment for the determination (it should be noted that the brown line is used by mistake for the S_c^{eff} evaluation at depths of $Z_c < Z_1$ in the former papers [3, 4]).

The following expression [3, 4] has been reported for the determination of S_c^{eff} at depths of $Z_c \geq Z_1$ using sets of a_1, b_1, and c_1 factors (see Table 1):

$$S_c^{eff}(Z_c, E) = a_1(E)\exp\left[b_1(E){Z_c}^{c_1(E)}\right]. \quad \text{(Eq. 1)}$$

For depths of $Z_c < Z_1$, this paper proposes the following expression:

$$S_c^{eff}(Z_c, E) = a'_1(E)\exp\left[b'_1(E){Z_c}^2\right], \quad \text{(Eq. 2)}$$

where we let $a'_1(E)$ be equal to the S_c^{eff} (0) field side at Z_c=0 determined using the above-described geometry of the fan beam coming out from the electron applicator, and then the value of $b'_1(E)$ is determined by setting

$$a'_1(E)\exp\left[b'_1(E){Z_1}^2\right] = a_1(E)\exp\left[b_1(E){Z_1}^{c_1(E)}\right]. \quad \text{(Eq. 3)}$$

Table 1 also lists sets of $a'_1(E)$ and $b'_1(E)$ values for the *KK* numbers (this paper also uses a simplified expression of S_c^{eff} (Z_c) for S_c^{eff} (Z_c, E) in case of taking a constant beam energy E beforehand). Figure 1 shows how the effective field side (S_c^{eff}) varies with depth (Z_c). As described above, Z_1 and Z_2 are specified depths used in the OAD datasets of the W-K paper (it should be emphasized that we can set $S_c^{eff}(0) \cong S_c^{eff}(Z_1)$; it seems that the W-K paper takes such a special Z_1 value for each beam energy (E)).

Table 2 Sets of the effective square field sides (S_c^{eff}) for each beam of (a), (b), (c), and (d) as described below:

Table 2a For the standard eMC dose-curves (step) of *KK*=1 & 2 (*E*=6 MeV), *KK*=3 & 4 (*E*=12 MeV), and *KK*=5 & 6 (*E*=18 MeV) using the direct electron beams.

E	*6 MeV*	*12 MeV*	*18 MeV*
A_{appl}	10×10 cm^2	10×10/14×14 cm^2	10×10 cm^2
SSD_{eff}	82.9 cm	91.5 cm	86.9 cm
S_c^{eff}	10.6 cm (Z_c=0 cm) 12.9 cm (Z_c=1 cm (= Z_1) 17.7 cm (Z_c=5 cm (=Z_2))	10.5 cm (Z_c=0 cm) 12.4 cm (Z_c=2 cm (= Z_1) 23.0 cm (Z_c=10 cm (=Z_2))	10.6 cm (Z_c=0 cm) 13.2 cm (Z_c=3 cm (= Z_1)) 27.9 cm (Z_c=15 cm (= Z_2))

Table 2b For the TPS eMC dose-curves (dot) of *KK*=7 & 8 (*E*=6 MeV), *KK*=9 & 10 (*E*=12 MeV), and *KK*=11 & 12 (*E*=18 MeV) using the direct electron beams.

E	*6 MeV*	*12 MeV*	*18 MeV*
A_{appl}	10×10 cm^2	10×10/14×14 cm^2	10×10 cm^2
SSD_{eff}	82.9 cm	91.5 cm	86.9 cm
S_c^{eff}	10.6 cm (Z_c=0 cm) 13.4 cm (Z_c=1 cm (=Z_1)) 17.8 cm (Z_c=5 cm (=Z_2))	10.5 cm (Z_c=0 cm) 12.4 cm (Z_c=2 cm (=Z_1)) 21.6 cm (Z_c=10 cm (=Z_2))	10.6 cm (Z_c=0 cm) 13.2 cm (Z_c=3 cm (=Z_1)) 28.2 cm (Z_c=15 cm (=Z_2))

Table 2c For the standard eMC dose-curves (step) of *KK*=13 & 14 (*E*=6 MeV), *KK*=15 & 16 (*E*=12 MeV), and *KK*=17 & 18 (*E*=18 MeV) using the direct-plus-indirect electron beams.

E	*6 MeV*	*12 MeV*	*18 MeV*
A_{appl}	10×10 cm^2	10×10/14×14 cm^2	10×10 cm^2
SSD_{eff}	82.9 cm	91.5 cm	86.9 cm
S_c^{eff}	10.6 cm (Z_c=0 cm) 13.4 cm (Z_c=1 cm (=Z_1)) 17.7 cm (Z_c=5 cm (=Z_2))	10.5 cm (Z_c=0 cm) 12.4 cm (Z_c=2 cm (=Z_1)) 25.8 cm (Z_c=10 cm (=Z_2))	10.6 cm (Z_c=0 cm) 13.2 cm (Z_c=3 cm (=Z_1)) 27.9 cm (Z_c=15 cm (=Z_2))

Table 2d For the TPS eMC dose-curves (dot) of *KK*=19 & 20 (*E*=6 MeV), *KK*=21 & 22 (*E*=12 MeV), and *KK*=23 & 24 (*E*=18 MeV) using the direct-plus-indirect electron beams.

E	*6 MeV*	*12 MeV*	*18 MeV*
A_{appl}	10×10 cm^2	10×10/14×14 cm^2	10×10 cm^2
SSD_{eff}	82.9 cm	91.5 cm	86.9 cm
S_c^{eff}	10.6 cm (Z_c=0 cm) 13.4 cm (Z_c=1 cm (=Z_1)) 17.8 cm (Z_c=5 cm (=Z_2))	10.5 cm (Z_c=0 cm) 12.4 cm (Z_c=2 cm (=Z_1)) 20.9 cm (Z_c=10 cm (=Z_2))	10.6 cm (Z_c=0 cm) 13.2 cm (Z_c=3 cm (=Z_1)) 28.5 cm (Z_c=15 cm (=Z_2))

2.3. Parallel beam depth-doses at infinite field

For the dose calculation for a given electron beam, the Gaussian pencil beam model uses a dataset of parallel beam depth-dose (D_∞) in an infinitely broad field. We have had experiences [3, 4] that the D_∞ datasets could reasonably be reconstructed for depths less than about the extrapolated range (R_p); however, not reasonably be reconstructed for depths beyond about the R_p range. The present paper proposes a reasonable procedure for it as follows:

Figure 2 shows a blue line expressing a raw set of D_∞ data for a given beam energy E, appearing unreasonable data at depths greater than $Z_c = Z_0(E)$ taking a dose of $a_0(E)$ at depth of $Z_0(E)$. Then this paper proposes a different set of D_∞ data at depths of $Z_c > Z_0(E)$ using a brown line as

$$F(Z_c, E) = a_0(E)\exp[-b_0(E)(Z_c - Z_0(E))^{0.7}]. \quad \text{(Eq. 4)}$$

It should be noted that the constant parameter-value of 0.7 is determined by examination of sets of OAD curves produced for all the beam energies of 6, 12, and 18 MeV, and that the value of $b_0(E)$ is determined by examination of a set of OAD curves of E under the constant 0.7-parameter, especially by taking into account the OAD curve at the depth of Z_2. Table 3 (composed of Tables 3a and 3b) lists datasets of $a_0(E)$, $b_0(E)$, and $Z_0(E)$ values (a) for the *direct electron* beams (*KK*=1-12) and (b) for the *direct-plus-indirect electron* beams (*KK*=13-24).

2.4. Calculation of depth-doses for fan beams

It should be emphasized that the dose calculation for the fan beams is performed using the same procedures as in the former papers of Refs. [3 and 4], only excepting: (i) the

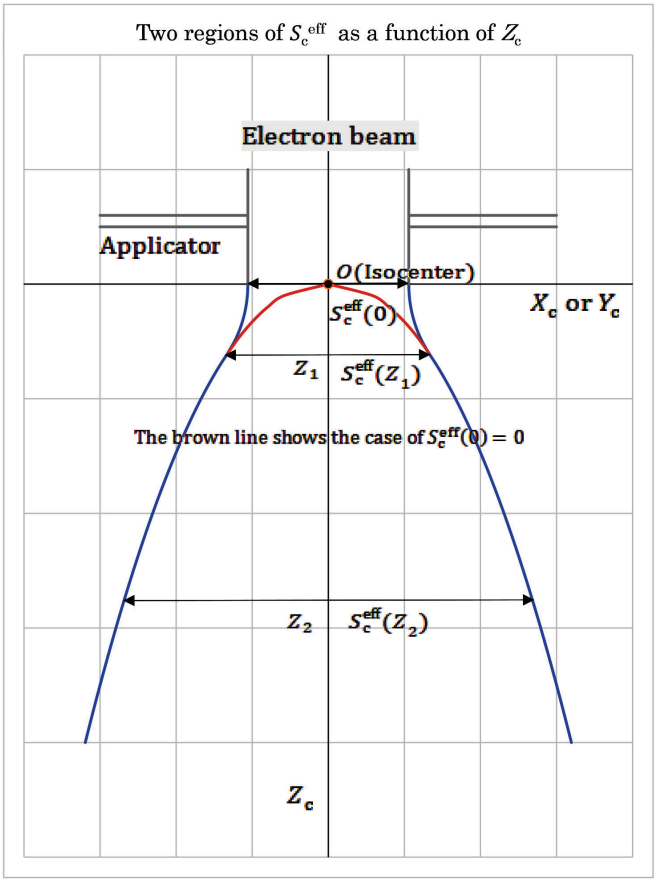

Figure 1 Two regions of S_c^{eff} as a function of Z_c. One is for $Z_c < Z_1$ and the other is for $Z_c \geq Z_1$. The blue lines are used in this study; on the other hand, the brown line takes in the former papers by mistake, showing $S_c^{eff}(0) = 0$.

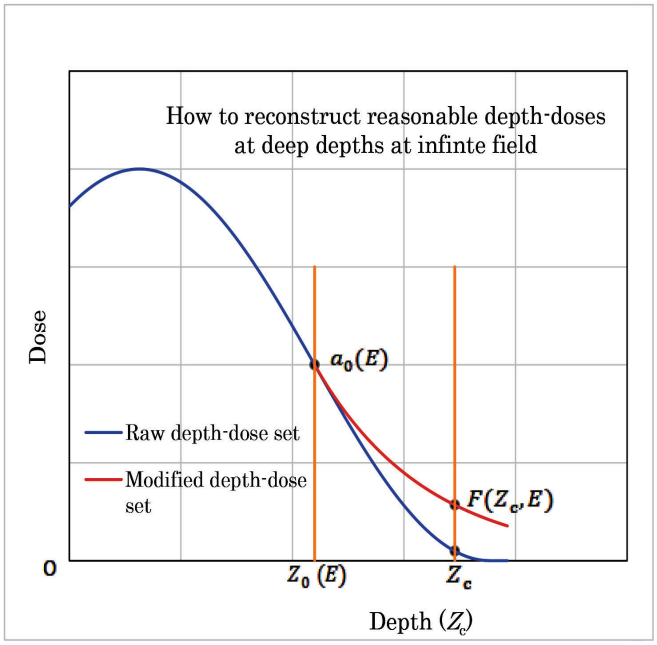

Figure 2 The blue line expresses a raw set of D_∞ data appearing unreasonable data at depths greater than $Z_c = Z_0(E)$ taking a dose of $a_0(E)$ for a given beam energy E. This paper proposes a different set of D_∞ data at depths of $Z_c > Z_0(E)$ using a brown line expressed by Eq. 4.

mathematical treatment for calculation of the effective field side (S_c^{eff}) for depths of $Z_c < Z_1$

using Eq. 2 (referring to Figure 1); and (ii) the mathematical treatment for calculation of the parallel beam dose dataset (D_{para}) of infinite field at deep depths using Eq. 4 (referring to Figure 2).

Table 3 Datasets of $a_0(E)$, $b_0(E)$, and $Z_0(E)$ used in Eq. 4 for (a) *KK*=1-12 (direct electron beams) and (b) for *KK*=13-24 (direct-plus-indirect electron beams), related with the beam energy (E), the applicator (A_{appl}), and the standard or TPS eMC (the italic "*figure numbers*" are used in the W-K paper [2]).

Table 3a For the direct electron beams (KK=1-12).

W-K datasets (KK=1-12)	E (MeV)	A_{appl} (cm²)	$a_0(E)$ (Gy/100 MU)	$b_0(E)$ (no unit)	$Z_0(E)$ (cm)
(i) Using the standard eMC (in *stepped* curves)					
KK=1 & 2 for *Supp. Fig.* 3(a)-(c)	6	10×10	8.36E-02	2.875	3.35
KK=3 & 4 for *Supp. Fig.* 5(a)-(c)	12	10×10/14×14	1.08E-02	0.530	7.00
KK=5 & 6 for *Supp. Fig.* 3(d)-(f)	18	10×10	1.30E-02	0.273	9.72
(ii) Using the TPS eMC (in *dotted* curves)					
KK=7 & 8 for *Supp. Fig.* 3(a)-(c)	6	10×10	8.88E-02	2.868	3.33
KK =9 & 10 for *Supp. Fig.* 5(a)-(c)	12	10×10/14×14	1.08E-02	0.582	7.00
KK=11 & 12 for *Supp. Fig.* 3(d)-(f)	18	10×10	1.41E-02	0.292	9.89

Results and discussion

Supplementary Figures (*Supp. Fig.*) 3-12 illustrate (a) & (b) DD datasets and (c) & (d) OAD datasets for E=6, 12, and 18 MeV beams, being partly compared with the corresponding dose datasets copied directly from the W-K eMC dose work (the standard or TPS eMC). For each DD or OAD dataset, we give a detailed explanation using the factors given in Figure 2 and given in Tables 1 and 2 as follows:

- *Supp. Fig.* 3 shows the case of the direct electron beams based on the standard eMC for each of the (a)-(d) diagrams with respect to *KK*=1 and 2 (E=6 MeV). It should be noted that the (a) and (b) diagrams express DD datasets, respectively, in a wide Z_c region and only in a deep Z_c region. In each of the (a) and (b) diagrams, the blue line expresses the doses of calculation, the set of gray marks expresses the doses copied from the W-K eMC dose datasets, the yellow line expresses the parallel-beam doses at infinite field, the brawn and blue marks express the doses of infinite field at Z_c=Z_2 and Z_c=$Z_0(E)$, respectively (Figure 2). On the other

Table 3b For the *direct-plus-indirect electron* beams (*KK*=13-24).

W-K datasets (KK=13-24)	*E (MeV)*	A_{appl} (cm^2)	$a_0(E)$ *(Gy/100 MU)*	$b_0(E)$ *(no unit)*	$Z_0(E)$ *(cm)*
(i) Using the standard eMC (in *stepped* curves)					
KK=13 & 14 for *Supp. Fig.* 3(a)-(c)	6	10×10	8.96E-02	2.922	3.36
KK=15 & 16 for *Supp. Fig.* 5(a)-(c)	12	10×10/14×14	3.01E-02	0.964	6.94
KK=17 & 18 for *Supp. Fig.* 3(d)-(f)	18	10×10	1.44E-02	0.290	9.91
(ii) Using the TPS eMC (in *dotted* curves)					
KK=19 & 20 for *Supp. Fig.* 3(a)-(c)	6	10×10	8.96E-02	2.922	3.36
KK=21 & 22 for *Supp. Fig.* 5(a)-(c)	12	10×10/14×14	3.77E-02	0.993	6.36
KK=23 & 24 for *Supp. Fig.* 3(d)-(f)	18	10×10	1.23E-02	0.246	9.88

hand, in each of the (c) and (d) diagrams, the solid lines express the OAD datasets of calculation, and the two sets of round marks express the OAD datasets copied from the W-K eMC dose datasets. It can be seen that the OAD datasets of calculation are reconstructed also by taking account of the balanced forms from shallow to deep depths and also by coinciding well with the W-K eMC dose datasets using Eqs. 1-4. It can be seen that much more accurate DD and OAD curves are yielded even at small Z_c regions, when compared with the results in Ref. [4] (this means that the S_c^{eff} function of Eq. 2 is reasonable).

- *Supp. Fig.* 4 shows the case of *KK*=3 and 4 (*E*=12 MeV) with the direct electron beams based on the standard eMC. The others are the same as in *Supp. Fig.* 3.
- *Supp. Fig.* 5 shows the case of *KK*=5 and 6 (*E*=18 MeV) with the direct electron beams based on the standard eMC. The others are the same as in *Supp. Fig.* 3.
- *Supp. Fig.* 6 shows the case of *KK*=7 & 8 (*E*=6 MeV) with the direct electron beams based on the TPS eMC. The others are the same as in *Supp. Fig.* 3.
- *Supp. Fig.* 7 shows the case of *KK*=9 & 10 (*E*=12 MeV) with the direct electron beams based on the TPS eMC. The others are the same as in *Supp. Fig.* 3.
- *Supp. Fig.* 8 shows the case of *KK*=11 & 12 (*E*=18 MeV) with the direct electron beams based on the TPS eMC. The others are the same as in *Supp. Fig.* 3.
- *Supp. Fig.* 9 shows the case of *KK*=13 & 14 (*E*=6 MeV) with the direct-plus-indirect electron beams based on the standard eMC. The others are the same as in *Supp. Fig.* 3.
- *Supp. Fig.* 10 shows the case of *KK*=15 & 16 (*E*=12 MeV) with the direct-plus-indirect electron beams based on the standard eMC. The others are the same as in *Supp. Fig.* 3.
- *Supp. Fig.* 11 shows the case of *KK*=17 & 18 (*E*=18 MeV) with the direct-plus-indirect electron beams based on the standard eMC. The others are the same as in *Supp. Fig.* 3.
- *Supp. Fig.* 12 shows the case of *KK*=19 & 20 (*E*=6 MeV) with the direct-plus-indirect electron beams based on the TPS eMC. The others are the same as in *Supp. Fig.*3.
- *Supp. Fig.* 13 shows the case of *KK*=21 & 22 (*E*=12 MeV) with the direct-plus-indirect electron beams based on the TPS eMC. The others are the same as in *Supp. Fig.*3.
- *Supp. Fig.* 14 shows the case of *KK*=23 & 24 (*E*=18 MeV) with the direct-plus-indirect electron beams based on the TPS eMC. The others are the same as in *Supp. Fig.*3.

From the present investigation, the following features have been observed:

Dose differences between the DD curve of finite field and that of infinite field become greater as the increase of the beam energy (*E*). This means that the range of laterally scattered electrons becomes greater with the increase of the beam energy (*E*). This phenomenon can be explained by the σ_z^p or σ_r function (Refs. 5 and 6).

The revised Gaussian-pencil-beam-model uses a mathematical σ_r expression, being reconstructed based on datasets of σ_z^p for *E* = 6,10,14, and 20 MeV as reported by Bruinvis *et al*. [5].

The three DD points of a_0 (*E*) for *E*=18 MeV in *Supp. Figs.* 8, 11, and 14 are respectively placed at a little wrong places. This fact has been found when writing this paper (we do not dare correct them in this paper).

The weak three points of the former papers of Refs. [3 and 4] regarding the calculated DD and OAD datasets, as noted in the introduction section, have been resolved.

Conclusion

To conclude this research report, we would like to conduct research on the development of the Gaussian pencil beam model when the phantom contains non-uniform materials and the beam entrance surface of the phantom is uneven.

Conflicts of interest

This study was carried out in collaboration with Technology of Radiotherapy Corporation, Tokyo, Japan. This sponsor had no control over the interpretation, writing, or publication of this work.

Supplementary data

Supplementary material associated with this article can be found at http://dx.doi.org/10.14312/2399-8172.2024-2.

Reference

[1] Wieslander E, Knöös T. A virtual linear accelerator for verification of treatment planning systems. Phys Med Biol. 2000; 45:2887–2896.

[2] Wieslander E, Knöös T. A virtual-accelerator-based verification of a Monte Carlo dose calculation algorithm for electron beam treatment planning in homogeneous phantoms. Phys Med Biol. 2006; 51:1533–1544.

[3] Iwasaki A, Terashima S, Kimura S, Sutoh K, Kamimura K, et al. A revised Gaussian pencil beam model for calculation of the in-water dose caused by clinical electron-beam irradiation. J Radiol Imaging. 2022; 6:1–9.

[4] Iwasaki A, Terashima S, Kimura S, Sutoh K, Kamimura K, et al. Further development of the preceding Gaussian-pencil-beam-model used for calculation of the in-water dose caused by clinical electron-beam irradiation. J Radiol Imaging. 2023; 7:1–4.

[5] Bruinvis IAD, Amstel AV, Elevelt AJ, Laarse RVD. Calculation of electron beam dose distributions for arbitrarily shaped fields. Phys Med Biol. 1983; 28:667–683.

[6] Khan FM, Gibbons JP. Khan's The physics of radiation therapy; 5th edition. Philadelphia, USA; 2014. Available from: https://solution.lww.com/book/show/446502.